IOP Conference Series: Materials Science and Engineering

Spectral element modelling of wave propagation in isotropic and anisotropic shell-structures including different types of damage

To cite this article: R T Schulte *et al* 2010 *IOP Conf. Ser.: Mater. Sci. Eng.* **10** 012065

Spectral element modelling of wave propagation in isotropic and anisotropic shell-structures including different types of damage

R. T. Schulte, C.-P. Fritzen, J. Moll

Institute of Mechanics and Control – Mechatronics, University of Siegen, Paul-Bonatz-Str. 9-11, 57076 Siegen, Germany

E-mail: schulte@imr.mb.uni-siegen.de

Abstract. During the last decades, guided waves have shown great potential for Structural Health Monitoring (SHM) applications. These waves can be excited and sensed by piezoelectric elements that can be permanently attached onto a structure offering online monitoring capability. However, the setup of wave based SHM systems for complex structures may be very difficult and time consuming. For that reason there is a growing demand for efficient simulation tools providing the opportunity to design wave based SHM systems in a virtual environment. As usually high frequency waves are used, the associated short wavelength leads to the necessity of a very dense mesh, which makes conventional finite elements not well suited for this purpose. Therefore in this contribution a flat shell spectral element approach is presented. By including electromechanical coupling a SHM system can be simulated entirely from actuator voltage to sensor voltage. Besides a comparison to measured data for anisotropic materials including delamination, a numerical example of a more complex, stiffened shell structure with debonding is presented.

1. Introduction

During the last decade many Structural Health Monitoring (SHM) approaches based on ultrasonic waves have been developed to detect structural damage like cracks or delaminations [1]. In case of shell structures, guided waves offer a great potential for health monitoring applications. Because of their propagation mechanism they interact strongly even with small damage. Guided waves can be excited and sensed by piezoelectric elements that are permanently attached onto the structure. This accounts for two major advantages: The elements are quite inexpensive compared to conventional NDT transducers and moreover the permanent installation enables the possibility of continuous monitoring.

Many research groups have developed SHM systems based on guided waves, but despite the aforementioned advantages and considerable efforts, few of these systems have accomplished the step from laboratory to real world application. The majority of these systems has a technology readiness level (TRL) is in the range between two and five of maximum nine. The obstacles preventing this transfer arise from different directions including regulation authorities (mainly in aircraft industry) and limited long-term experience with the systems. Although it is widely accepted that SHM systems can offer maintenance and design benefits (see e.g. [2]) quantification of the financial benefit for the end-user is difficult.

Another important reason seems to be the complexity of the technology itself: To set up an SHM system for a real-world structure, a deep knowledge of wave propagation phenomena including effects of damping and wave scattering is necessary. The development-process for an optimized SHM system may be very laborious and costly, because the capabilities of most approaches strongly depend on an adequate choice of parameters like excitation signals, damage evaluation algorithms, actuator/sensor types and actuator/sensor distribution. Usually, the optimization by trial and error of all these parameters that is necessary for successful monitoring of complex structures requires lots of tedious and costly pretests. In a comparative study, Herszberg et al. stated that the performance of all available techniques has to be improved to be seriously considered for practical usage [3].

For this reason there is a growing interest in accurate and efficient simulation tools to enable virtual SHM system design. This is expected to shorten time and cost of necessary pretests and to improve the adaptation of SHM systems from laboratory environment to in-service structures.

For the modelling of wave propagation phenomena a variety of methods is utilized. Among others the finite difference method (FDM) [3], the pseudospectral method (PSM) [4], the finite element method (FEM) [5], the boundary element method (BEM) [6] and the local interaction simulation approach (LISA) [7] are used. To detect small damage generally high frequency excitation signals are required because the size of the defects should be similar to the wavelength of the propagating waves. Therefore, a very dense finite element mesh is inevitable to accurately simulate the wave propagation including the effects of wave scattering at structural discontinuities. Hence, conventional finite element simulation becomes computationally very inefficient. Finite difference methods suffer from numerical dispersion and difficulties arise when implementing boundary conditions [8].

A more promising method is the spectral element method that was first proposed by Patera [9]. It combines the accuracy of the global pseudospectral method with the flexibility of the FEM. However, using the spectral element method (SEM) is not widespread in the context of high frequency guided waves modelling. Kudela and Ostachowicz simulate propagating waves in beams and delaminated plates with spectral plate elements [10] and Peng et al. model in-plane waves in plates with 3D spectral elements [11].

While modelling of guided wave in theory requires a full 3D model, a 2D approach can be used for thin shells with certain accuracy. This contribution presents the formulation of spectral elements for flat shells based on first order shear deformation (FSDT) theory. The effect of symmetrical material layup on the element matrices and the numerical efficiency is discussed. Moreover the utilization of a 2D approach is justified by comparison of dispersion curves to exact 3D solutions.

To be able to handle composite material - which usually exhibits a relatively large amount of material damping - direction-dependent attenuation factors can be implemented. By incorporating the contributions of piezoelectric elements, the presented methodology allows the complete simulation of wave-based SHM systems from actuator voltage signal up to sensor output voltage.

The accuracy of the approach is demonstrated by comparing numerical results to experimental data for composite plates including a delamination. Additionally a numerical example of propagating waves in a stiffened shell structure is shown and the effect of stringer debonding is analyzed.

2. Spectral elements for flat shells

The Gauss-Lobatto-Legendre (GLL) spectral element discretization based upon quadrangular elements is quite similar to classical FE in many points, but few variations in construction result in significantly improved element properties. The procedure is as follows: a mesh of n_{el} non-overlapping elements is defined on the domain. These elements Ω^e are subsequently mapped individually to a reference element Ω^{ref}: $\xi \in [-1,1] \times \eta \in [-1,1]$. On each element a set of GLL nodes is defined. Within the reference element these nodes are the (N+1) roots of the polynomials

$$(1-\xi^2)P'_{N-1}(\xi)=0 \qquad \text{and} \qquad (1-\eta^2)P'_{N-1}(\eta)=0\,, \tag{1}$$

where P'_{N-1} denotes the first derivative of the (N-1)-th order Legendre polynomial. In contrast to classical lower order finite elements the distribution of nodes is irregular. The spectral shell element is based on FSDT with out-of-plane displacement w, independent rotations θ_x and θ_y and in-plane displacements u and v. The basic equations of motions resulting from this theory can be found in many textbooks, see e.g. [13]. The rotation about local z-axis θ_z is not needed to formulate the membrane behaviour of the element, but to be able to transform the element matrices in space between local and global coordinates, it is meaningful to introduce this additional degree of freedom (dof). It is possible to use elements with explicit θ_z-dof but this would complicate the matters unnecessarily. Instead, small artificial values for the stiffness and mass of this dof are defined, see [14].

On the nodal base defined above, Lagrange interpolation polynomials can be used as shape functions, leading to an expression of the displacement field in the following form

$$\begin{bmatrix} w(\xi,\eta) \\ \theta_x(\xi,\eta) \\ \theta_y(\xi,\eta) \\ u(\xi,\eta) \\ v(\xi,\eta) \end{bmatrix} = \sum_{i=1}^{N+1}\sum_{j=1}^{N+1} \Psi_{ij}(\xi,\eta)\mathbf{q}_{ij}^{(e)} = \sum_{i=1}^{N+1}\sum_{j=1}^{N+1} \psi_i(\xi)\cdot\psi_j(\eta) \begin{bmatrix} \hat{w}(\xi_i,\eta_j) \\ \hat{\theta}_x(\xi_i,\eta_j) \\ \hat{\theta}_y(\xi_i,\eta_j) \\ \hat{u}(\xi_i,\eta_j) \\ \hat{v}(\xi_i,\eta_j) \end{bmatrix}. \tag{2}$$

Here $\psi_i(\xi)$ denotes the i-th 1-D Lagrange interpolation function. The nodal degrees of freedom are labelled with a hat and arranged in vector $\mathbf{q}$. By utilizing this kind of shape functions based on the GLL-nodes, the highest interpolation accuracy is achieved [15]. This leads to the advantage, that only five to six nodes (depending on the degree of the interpolation polynomial) per shortest wavelength of the excited frequency range are necessary to capture the structural behaviour with the same accuracy as 15-30 nodes, which are needed using lower order FE [16]. Three typical shape functions are shown in figure 1 indicating that each shape function is exactly one at one node and zero at all other nodes.

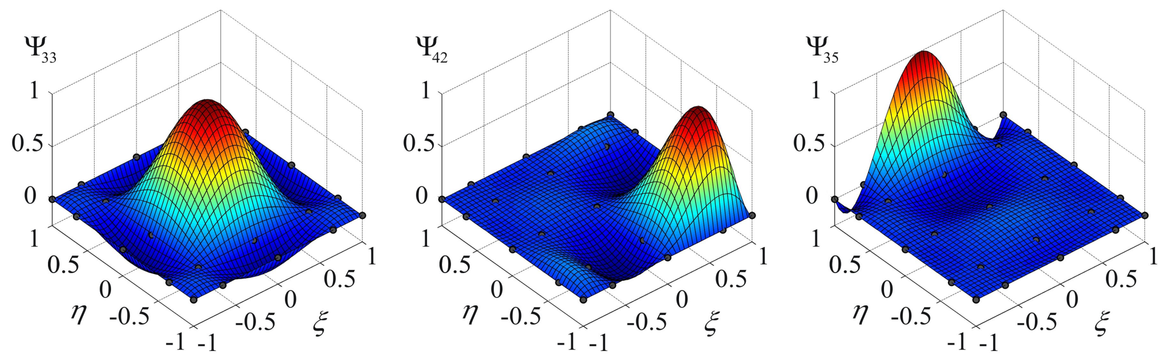

Figure 1. Example of three typical shape functions of a spectral element with 25 nodes

The derivation of weak form and assembly of mass- and stiffness matrix follows standard FE procedures. The element mass- and stiffness matrices can be calculated as

$$\mathbf{M}^{(e)} = \iint_{\Omega^e} [\mathbf{\Psi}(x,y)]^T\ \mathbf{H}\,\mathbf{\Psi}(x,y)\det(\mathbf{J})d\Omega \approx \sum_{i=1}^{N+1}\sum_{j=1}^{N+1} \overline{w}_i\ \overline{w}_j \left[\mathbf{\Psi}(x_i,y_j)\right]^T\ \mathbf{H}\,\mathbf{\Psi}(x_i,y_j)\ \det(\mathbf{J}), \tag{3}$$

$$\mathbf{K}^{(e)} = \iint_{\Omega^e} [\mathbf{B}(x,y)]^T\ \mathbf{D}\ \mathbf{B}(x,y)\ \det(\mathbf{J})\ d\Omega \approx \sum_{i=1}^{N+1}\sum_{j=1}^{N+1} \overline{w}_i\ \overline{w}_j \left[\mathbf{B}(x_i,y_j)\right]^T\ \mathbf{D}\ \mathbf{B}(x_i,y_j)\ \det(\mathbf{J}). \tag{4}$$

where $\overline{w}$ is an integration weight, $\mathbf{J}$ is the Jacobi matrix of the mapping and $\mathbf{B}$ is the strain-displacement matrix and is given in the appendix. Matrix $\mathbf{H}$ contains the material inertia terms and $\mathbf{D}$ is the material stiffness matrix, containing the elasticity constants:

$$\mathbf{H}=\begin{bmatrix} I_0 & 0 & 0 & 0 & 0 \\ 0 & I_2 & 0 & 0 & -I_1 \\ 0 & 0 & I_2 & I_1 & 0 \\ 0 & 0 & I_1 & I_0 & 0 \\ 0 & -I_1 & 0 & 0 & I_0 \end{bmatrix} \quad \text{and} \quad \mathbf{D}=\begin{bmatrix} D_{11} & D_{12} & D_{16} & 0 & 0 & B_{11} & B_{12} & B_{16} \\ D_{12} & D_{22} & D_{26} & 0 & 0 & B_{12} & B_{22} & B_{26} \\ D_{16} & D_{26} & D_{66} & 0 & 0 & B_{16} & B_{26} & B_{66} \\ 0 & 0 & 0 & \kappa A_{55} & \kappa A_{45} & 0 & 0 & 0 \\ 0 & 0 & 0 & \kappa A_{45} & \kappa A_{44} & 0 & 0 & 0 \\ B_{11} & B_{12} & B_{16} & 0 & 0 & A_{11} & A_{12} & A_{16} \\ B_{12} & B_{22} & B_{26} & 0 & 0 & A_{12} & A_{22} & A_{26} \\ B_{16} & B_{26} & B_{66} & 0 & 0 & A_{16} & A_{26} & A_{66} \end{bmatrix}. \quad (5)$$

A_{ij}, B_{ij} and D_{ij} are extensional-, coupling- and bending coefficients respectively and κ is a shear correction factor. With the element thickness h^e the inertia terms are defined as

$$I_0=\int_{h^e}\rho(z)\,dz\,, \quad I_1=\int_{h^e}z\,\rho(z)\,dz \quad \text{and} \quad I_2=\int_{h^e}z^2\rho(z)\,dz\,. \quad (6)$$

For the general case of anisotropic laminates, this formulation leads to an optimally concentrated, but non-diagonal mass matrix because of the coupling of in-plane and rotational dofs by I_1. Fortunately in almost every application, laminates with symmetrical layup are used and in this case I_1 and also the coupling coefficients B_{ij} vanish. In this situation the discrete orthogonality of the shape functions in conjunction with the Gauss-Lobatto integration rule to evaluate the numerical integration in equation (3) leads to a diagonal mass matrix **M**.

In contrast to metallic materials, most CFRP or GFRP laminates exhibit a comparatively large amount of material damping. To be able to incorporate this behaviour into the simulation approach, a material damping matrix is defined on element level. Often proportional damping is assumed for reasons of simplicity, but within this contribution another approach is used: Different damping coefficients are defined for in-plane and out of-plane behaviour and for the fibre- and the transverse direction of each layer. For the k-th layer this leads to the following matrix structure:

$$\mathbf{C}_{mat}^{(k)}=\begin{bmatrix} \left(C_{\theta f}^{(k)}+C_{\theta m}^{(k)}\right)/2 & 0 & 0 & 0 & 0 \\ 0 & C_{\theta l}^{(k)} & 0 & 0 & 0 \\ 0 & 0 & C_{\theta f}^{(k)} & 0 & 0 \\ 0 & 0 & 0 & C_f^{(k)} & 0 \\ 0 & 0 & 0 & 0 & C_m^{(k)} \end{bmatrix}. \quad (7)$$

After transforming this matrix to the laminate coordinate system the damping matrix $\mathbf{C}^{(e)}$ is summed up from the contributions of each layer weighted by its thickness, leading to a material damping matrix $\mathbf{C}_{mat}$. The element damping matrix can be constructed similar to the mass matrix:

$$\mathbf{C}^{(e)}=\iint_{\Omega^e}[\mathbf{\Psi}(x,y)]^T\,\mathbf{C}_{mat}\,\mathbf{\Psi}(x,y)\det(\mathbf{J})d\Omega\approx\sum_{i=1}^{N+1}\sum_{j=1}^{N+1}\overline{w}_i\,\overline{w}_j\left[\mathbf{\Psi}(x_i,y_j)\right]^T\mathbf{C}_{mat}\,\mathbf{\Psi}(x_i,y_j)\,\det(\mathbf{J}). \quad (8)$$

For an arbitrary laminate layup the damping matrix may contain off-diagonal elements. In this case it is recommended to use some kind of diagonalization scheme.

After the assembly of all elements, this results in a linear system of 2nd-order differential equations that is very similar to a dynamic system resulting from conventional FE but with the advantageous property of diagonal mass- and damping matrices for laminates with symmetrical layup:

$$\mathbf{M}\,\ddot{\mathbf{q}}+\mathbf{C}\,\dot{\mathbf{q}}+\mathbf{K}\,\mathbf{q}=\mathbf{F}\,. \quad (9)$$

3. Electromechanical coupling and solution of the system of equations

In active guided-wave based SHM systems propagating waves are introduced by applying a voltage to a PZT element (indirect piezoelectric effect). In a similar manner the direct piezoelectric effect is used to sense the propagating waves at PZT sensors. These electro-mechanical coupling processes have to be incorporated within the simulation framework. In principle this could be achieved by formulating piezoelectric shells with additional electrical dofs, see e.g. [17].

This strategy is avoided here, because the size of the resulting systems should be kept as small as possible for reasons of efficiency. Instead, the coupling is performed semi-analytically. Assuming isotropic piezoelectric actuators, the magnitude of the induced line forces and line moments at the edges of a rectangular PZT actuator patch that is bonded onto the surface of a flat shell structure (actuator equation) can be expressed following as [18]

$$N_x^{pzt} = N_y^{pzt} = \frac{-E_{pzt} h_{pzt}}{1-\nu_{pzt}} \frac{d_{31}}{h_{pzt}} V_{pzt} \quad \text{and} \quad M_x^{pzt} = M_y^{pzt} = -\frac{1}{8} \frac{E_{pzt}}{1-\nu_{pzt}} \left(4\left(\frac{h}{2} + h_{pzt}\right)^2 - h^2 \right) \frac{d_{31}}{h_{pzt}} V_{pzt} \tag{10}$$

Here, h denotes the plate thickness, h_{pzt} is the piezo element thickness, d_{31} is a piezo-electric strain constant, E_{pzt} and ν_{pzt} are the Young's modulus and the Poisson's ratio of the PZT patch and V_{pzt} denotes the applied voltage. Using equation (10) it is straight forward to compute generalized actuator forces for any given voltage signal and add these forces to the vector of applied external forces **F** at the right hand side of equation (9).

A sensor equation is developed for orthotropic situations in [19] and is used to calculate the output charge $Q(t)$:

$$Q(t) = -\iint_S (F + \varepsilon_{33}^X E_3)\,dxdy + z_k \iint_S G\,dxdy\,, \tag{11}$$

where F and G are defined as

$$F(x,y) = e_{31}\frac{\partial u}{\partial x} + e_{32}\frac{\partial v}{\partial y} \quad \text{and} \quad G(x,y) = e_{31}\frac{\partial \theta_y}{\partial x} + e_{32}\frac{\partial \theta_x}{\partial y}\,. \tag{12}$$

The charge depends on the strain in the piezo patch, as can be seen in equation (12), where e_{31} and e_{32} are coupling coefficients. Using these equations avoids to add further degrees of freedom to the system. The strains can be calculated analytically using the strain-displacement matrix **B**. Effects of shear-lag can easily be implemented by loss factors. Besides these coupling equations, the contributions of the PZT patches to the local mass, stiffness and damping properties of the structure should be incorporated for an accurate model. In most cases the patches are attached onto just one side of a shell structure, resulting in coupling contributions of in-plane and out-of-plane dofs. Then the mass matrix of the corresponding elements has some off-diagonal terms that has to be kept in mind for the system solution. In case of thin PZTs in comparison to the structural thickness, these contributions may be neglected.

For the solution of the resulting system (equation (9) the central difference scheme can be employed. In case of fully diagonal mass- and damping matrices, the resulting equations can be solved without matrix decomposition, which is numerically very efficient. If several elements with off-diagonal terms in the mass matrix exist, an efficient solution can be found by dividing the system into two parts: the first, usually small part contains those rows and columns with off-diagonal terms and the second, usually much larger part with the remaining terms. Only for the first part, a matrix decomposition is necessary. So even in case of several elements with non-symmetrical layup, the resulting scheme is much faster than a conventional FE approach. For a given input voltage signal, the external forces can be calculated and the system can be solved for the displacements. The output charge from equation (11) can be calculated and easily transferred to sensor output voltage by treating the PZT as a parallel plate capacitor.

4. Dispersion curves based on FSDT– comparison to exact 3D solutions

Because of the usage of 2D first order shear deformation theory (FSDT), the proposed flat shell spectral element model is not able to account for the exact 3D particle motion of guided waves. Nevertheless up to a certain frequency range, the FSDT can be used to approximate guided waves quite accurately. A useful criterion to evaluate the application range is a comparison of dispersion curves derived from governing equations of motion of FSDT to exact solutions of 3D theory of elasticity. The dispersion curves based on FSDT are derived by inserting the assumed propagating waves for all dofs in the form of

$$q(x,y,t) = q_0 \cdot e^{-ikx\cos\beta} e^{-iky\sin\beta} e^{-i\omega t} \tag{14}$$

into the equations of motion, where q denotes each dof, q_0 is the amplitude, k is the wave number and β is the propagation angle. This leads to a system of equations that can be solved for k. Afterwards group- and phase velocities can be calculated. In figure 2(a) and 2(b) these velocities of the different wave modes are plotted over the frequency for a 2mm thick aluminium plate.

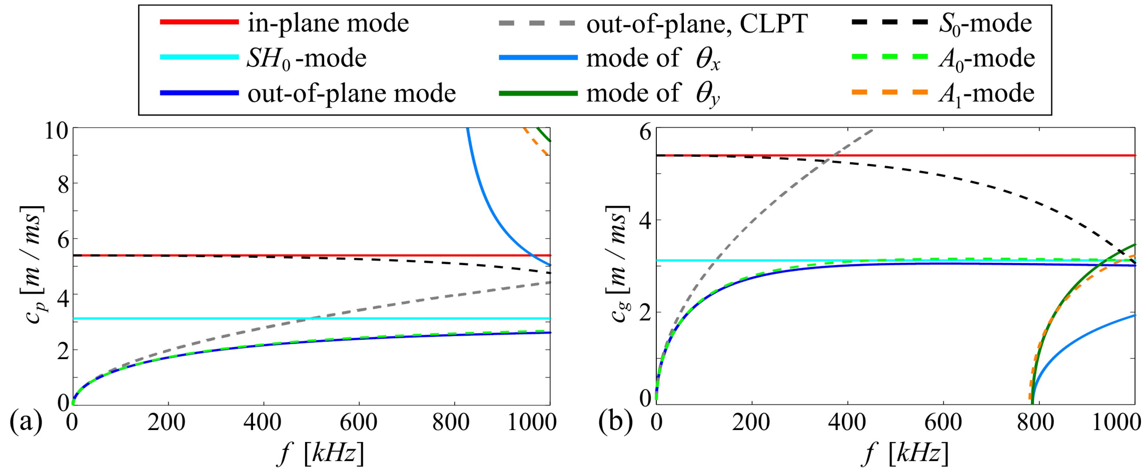

Figure 2. Velocities of different wave modes in an aluminium plate; comparison of plate theories to exact 3D solutions: (a) phase velocity and (b) group velocity

As can be noticed from figure 2 the in-plane mode of FSDT is not dispersive. However, up to 400kHz – that corresponds to a frequency-thickness product of 0.8MHzmm – the error in comparison to group velocity of S_0-mode is below 3%. Just as well is the conformity of out-of-plane mode and A_0-mode. The higher order modes are stated for completeness, but the further SEM models will concentrate on the fundamental modes only. The group velocity of out-of-plane mode of classical laminated plate theory (CLPT) shows large deviation from A_0-mode velocity beginning from 40kHz, justifying that CLPT cannot be used for higher frequencies.

5. Simulation of wave propagation in anisotropic structures with delaminations

For anisotropic materials besides the dispersion curves the direction-dependent velocities at constant frequency are quite interesting for the setup of a SHM system. These can be calculated using a similar approach as for the dispersion curves and compared to measured group velocities. The calculation process is very fast, which allows to cover a large space of material parameters in a limited amount of time. Hence, an efficient model-updating can be performed, because it is not necessary to run lots of SEM simulations. An example of this approach for a 1.45mm thick woven GFRP plate with high anisotropy is demonstrated in figure 3. The plate (figure 3(a)) and the calculated group velocities of the different modes (figure 3(b)) are shown in comparison to some measured values (red circles, only for S_0-mode). In figure 3(c) measured and simulated sensor signals for actuation of P5 with a five cycle burst signal of 100kHz centre frequency are compared. The cuspidal regions of the SH_0-mode indicate preferred energy transport in these directions for this wave mode. This behaviour is typical for many anisotropic laminates, see e.g. [21].

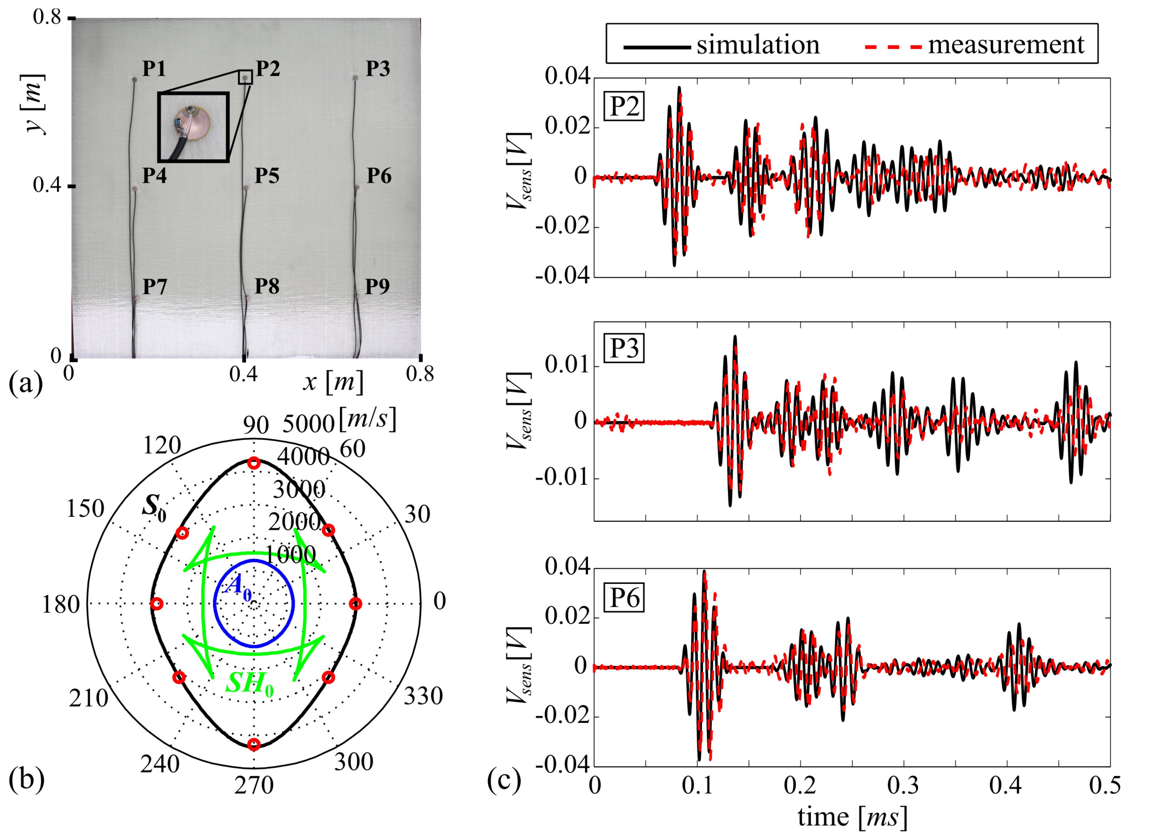

Figure 3. GFRP-plate: (a) setup, (b) updated group velocity curves and (c) comparison of SEM simulation and measured data; centre frequency of excitation is 100kHz.

The above example that is presented to demonstrate the SEM simulation capabilities for anisotropic structures is a single layer woven material. For that reason an impact event leads to some kind of destruction, but cannot cause a delamination. To demonstrate the simulation capabilities regarding delaminations, a different plate is analysed. This CFRP plate is made of 16 equal layers resulting in a total thickness of 4.2mm with a stacking of $[0\ 90\ -45\ 45\ 0\ 90\ -45\ 45]_s$. Nominal material parameters of the UD layers are the following: E_1=155GPa, E_2=8.5GPa, G_{12}= G_{13}=G_{23}=4GPa. The density is about 1600kg/m^3. The left part of figure 4 shows the plate of approximately 500mm x 500mm instrumented with nine PZTs. After several measurements in undamaged state, a low velocity impact with an energy of 15J is introduced between PZTs 5 and 2. The resulting delamination area is measured using an ultrasonic transducer and is additionally drawn into figure 4.

Within the spectral element model the delaminated area is simulated by using separated upper and lower elements as sketched on the right hand side of figure 4. It is worth to notice that those elements have no longer a symmetrical layup, so additional coupling between in-plane and out-of-plane modes may occur. Moreover the midplane of the delaminated layer has an offset a towards the midplane of undamaged structure. Contact between upper and lower elements in the delaminated area is neglected within this study. A comparison of modelled and measured sensor data for an excitation of P5 with centre frequency 60kHz is shown in figure 5. A satisfactory agreement for the undamaged case and the effect of delamination is demonstrated. The simulation shows the same behaviour as the measured data, which is a very small change in the S_0-mode and a larger time-shift in the A_0-mode at sensor P2.

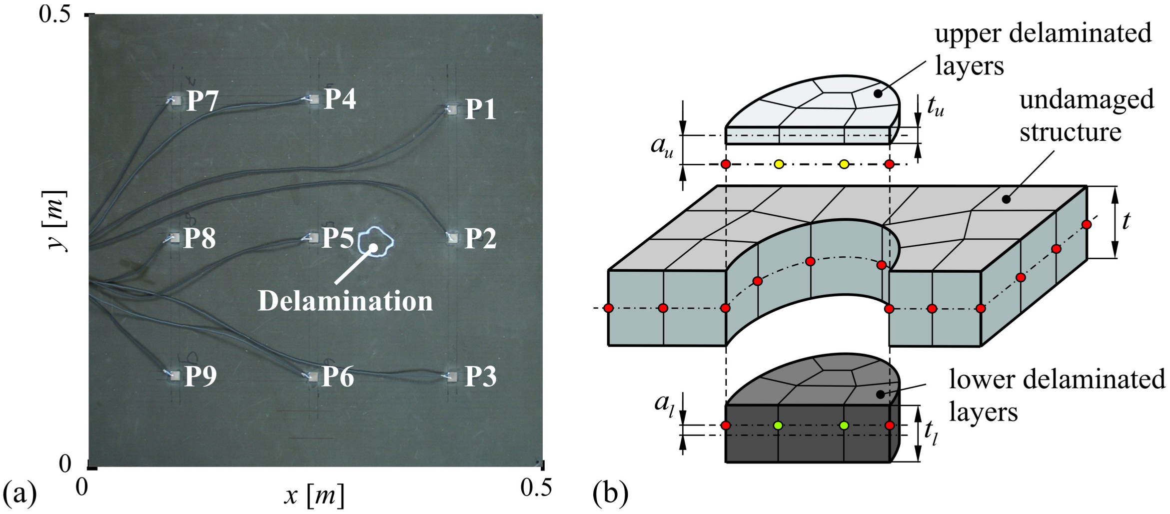

Figure 4. (a) CFRP-plate with delamination and (b) schematic diagram of delamination model.

The paths to the other sensors for actuating P5 show just minor differences, because the direct wave packages do not travel through the delaminated area. Similar, but smaller differences can be found for actuator-sensor paths P6-P1 and P4-P3 or the other way round.

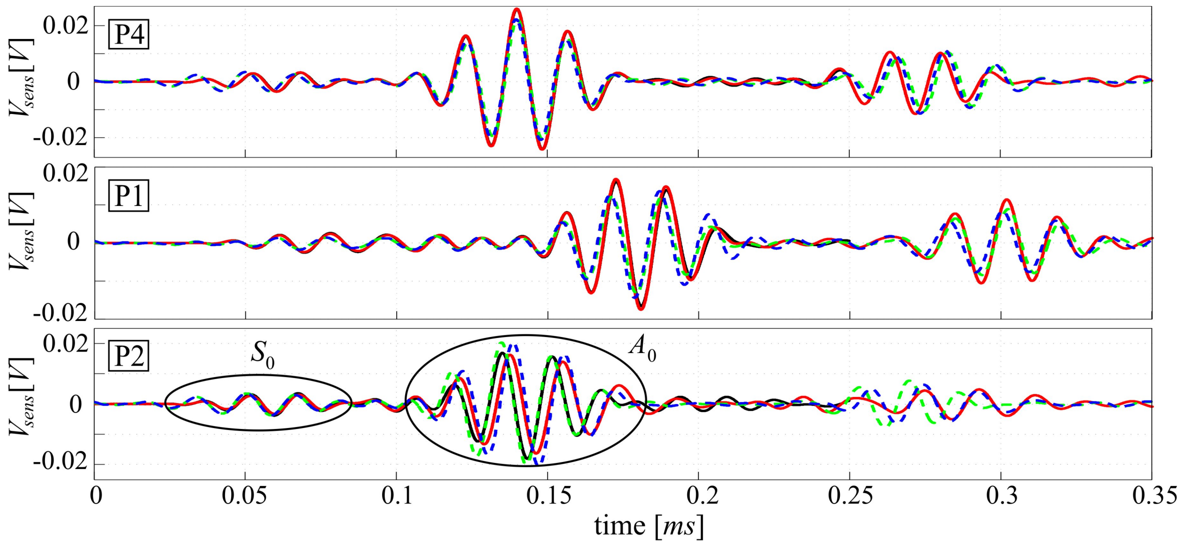

Figure 5. Comparison of simulated (solid lines) and measured (dashed lines) sensor data for undamaged (black and green) and delaminated (red and blue) case. Actuator is PZT 5.

6. SEM modelling of a stiffened panel with stringer debonding

To demonstrate a possible use case of the presented modelling approach, the numerical model of a stiffened panel is considered. The model consists of a base plate of thickness 2mm with three stiffeners. Isotropic material properties of aluminium are used. The stiffener in the middle is assumed to be T-shaped and perfectly bonded to the structure in the undamaged case. This results in an increased thickness of 3mm for some elements on both sides of the stiffener, see the additional lines in figure 6(b). The red coloured PZT is actuated using a three cycle tone burst of 75kHz. A serious damage case in real aircraft structures is stiffener debonding. For that reason a debonding is simulated in a small area close to the middle of the stiffener.

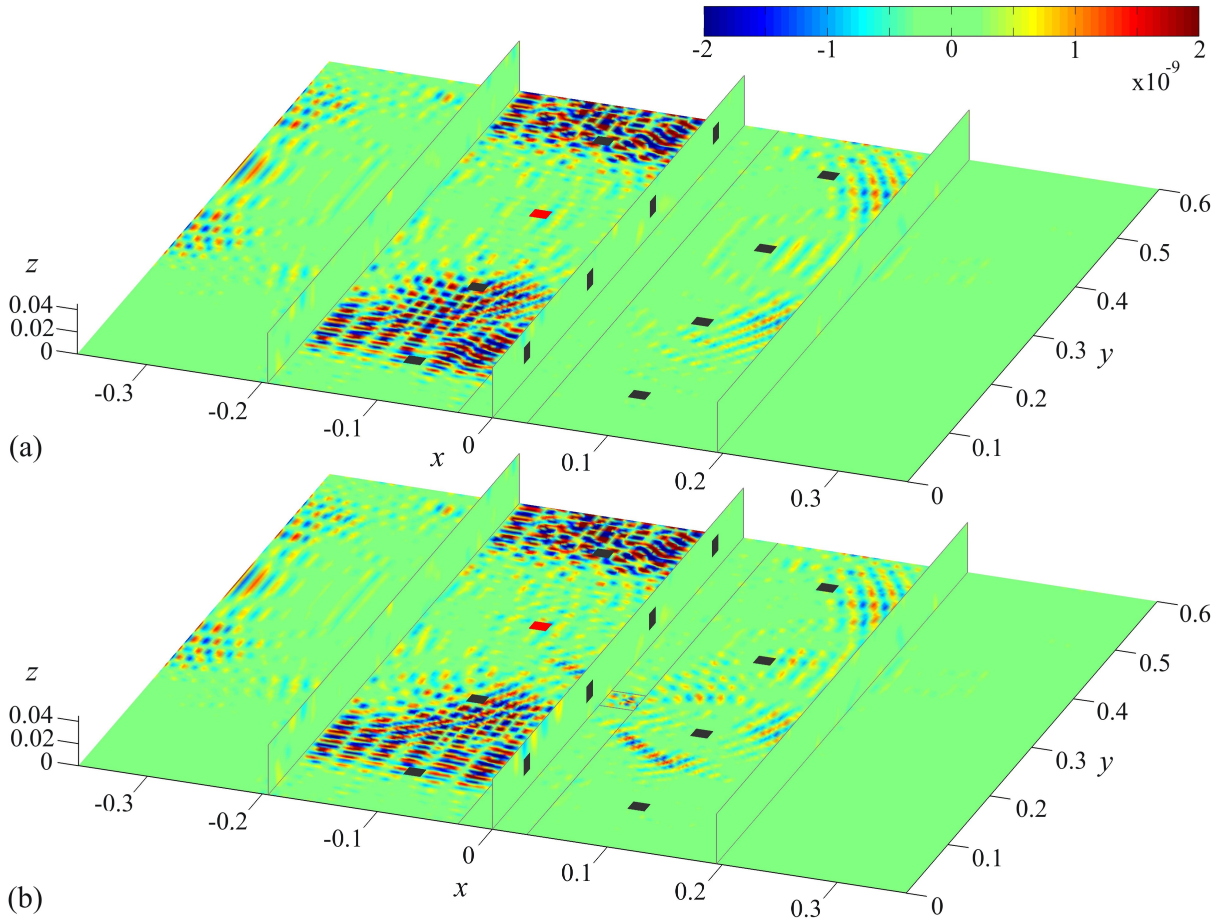

Figure 6. *z*-displacement of waves in a stiffened panel, (a) undamaged and (b) with stiffener debonding. Additional wave packages passing the stiffener at the debonded area can be noticed.

In figure 6 snapshots of the *z*-displacement of the induced waves at t=0.17ms for the undamaged and debonded cases are shown. While the main energy of the out-of-plane wave remains inside the area between two stiffeners, comparison of both snapshots clearly indicates several additional wave packages that can pass the stiffener in the debonded area. The amplitude of these wave packages is relatively large in comparison to the waves passing the stiffener in the undamaged case. The additional energy can be sensed in the adjacent area indicating this type of damage.

7. Conclusions

Modelling of guided wave-based SHM systems for thin shells has been presented. The proposed flat shell spectral element that is based on FSDT offers several advantageous features compared to conventional finite elements regarding accuracy and numerical efficiency. By implementing electromechanical coupling, the entire SHM system including actuating and sensing waves can be simulated. An approach to implement material damping is presented to be able to cover the strong attenuation of composite materials.

The capabilities of the model are demonstrated by comparison with measured data for two examples, including the effect of a delamination, which is modelled as separated upper and lower element layers. A possible use case of the proposed model within the development of SHM systems for more complex structures is demonstrated by analysing a panel with stiffener debonding. The effect of the debonding on the out-of-plane waves that are strongly isolated by the stiffeners is clearly seen. The generated data could be used as input for the development of advanced localization algorithms.

References

[1] Giurgiutiu V 2007 *Structural Health Monitoring with Piezoelectric Wafer Active Sensors* (San Diego: Academic Press)
[2] Schmidt H J, Telgkamp J and Schmidt-Brandecker B. 2004 *Proc. of the 2nd European Workshop on Structural Health Monitoring* (Munich, Germany) 11-18
[3] Herszberg I, Bannister M, Buderath M, Li M, Saenz E, Whittingham B. and Zhou Z 2008 *Proc. of the 4th European Workshop on Structural Health Monitoring* (Cracow, Poland) 43-50
[4] Graves R W 1996 *Bull. Seismol. Soc. Am.* **86** (4) 1091-1106
[5] Fornberg B 1987 *Geophys.* **52** 483-501
[6] Zienkiewicz O W, Taylor R L and Zhu J Z 2005 *The finite element method* 6th ed (Oxford: Elsevier Butterworth-Heinemann)
[7] Cho Y and Rose J L 1996 *J. Acoust. Soc. Am.* **99** 2079-2109
[8] Delsanto P P, Schechter R S and Mignogna R B 1997 *Wave Motion* **26** 329-339
[9] Komatitsch D, Martin R, Tromp J, Taylor M A and Wingate B A 2001 *J. Comp. Acoust.* **9** (2) 703-718
[10] Patera A T 1984 *J. Comput. Phys.* **54** 468-488
[11] Kudela P and Ostachowicz W 2009 *Mech. Adv. Mater. Struct.* **16** 174-187
[12] Peng H, Meng G and Li F 2008 *J. Sound Vib.* **320** 942-954
[13] Reddy J N 2004 *Mechanics of Laminated Composite Plates and Shells: Theory and Analysis* (Boca Raton: CRC)
[14] Bathe K-J 1986 *Finite-Element-Methoden* (Berlin: Springer)
[15] Pozrikidis C 2005 *Introduction to Finite and Spectral Element Methods using Matlab®* (CRC)
[16] Seriani G and Priolo E 1994 *Finite Elem. Anal. Des.* **16** 337-348
[17] Lammering R and Mesecke-Rischmann S 2003 *Smart Mater. Struct.* **12** (6) 904-913
[18] Banks H T, Smith R C and Wang Y 1996 *Smart material structures, modelling, estimation and control* (Paris: Wiley)
[19] Yang S and Ngoi B 1999 *Smart Mater. Struct.* **8** 411-415
[20] Calomfirescu M 2008 *Lamb Waves for Structural Health Monitoring in Viscoelastic Composite Materials* (Dissertation, Faserinstitut Bremen)
[21] Royer D and Dieulesaint E 2000 *Elastic Waves in Solids I* (Berlin: Springer)

Appendix

For slightly curved shells the strain-displacement matrix **B** used in equation (4) can be stated as

$$\mathbf{B}_{ij} = \begin{bmatrix} 0 & 0 & -\frac{\partial \Psi_{ij}}{\partial x} & 0 & 0 \\ 0 & \frac{\partial \Psi_{ij}}{\partial y} & 0 & 0 & 0 \\ 0 & \frac{\partial \Psi_{ij}}{\partial x} & -\frac{\partial \Psi_{ij}}{\partial y} & 0 & 0 \\ \frac{\partial \Psi_{ij}}{\partial x} & 0 & 1 & 0 & 0 \\ \frac{\partial \Psi_{ij}}{\partial y} & -1 & 0 & 0 & 0 \\ \frac{\partial \Psi_{ij}}{\partial x} \cdot \frac{\partial z_0}{\partial x} & 0 & 0 & \frac{\partial \Psi_{ij}}{\partial x} & 0 \\ \frac{\partial \Psi_{ij}}{\partial y} \cdot \frac{\partial z_0}{\partial y} & 0 & 0 & 0 & \frac{\partial \Psi_{ij}}{\partial y} \\ \frac{\partial \Psi_{ij}}{\partial x} \cdot \frac{\partial z_0}{\partial y} + \frac{\partial \Psi_{ij}}{\partial y} \cdot \frac{\partial z_0}{\partial x} & 0 & 0 & \frac{\partial \Psi_{ij}}{\partial y} & \frac{\partial \Psi_{ij}}{\partial x} \end{bmatrix}. \tag{A.1}$$